Brief Reports

Brief Reports are accounts of completed research which, while meeting the usual **Physical Review** *standards of scientific quality, do not warrant regular articles. A Brief Report may be no longer than four printed pages and must be accompanied by an abstract. The same publication schedule as for regular articles is followed, and page proofs are sent to authors.*

Solitary-wave dynamics in extrinsic semiconductors under dc voltage bias

Inma R. Cantalapiedra
Universidad Politécnica de Barcelona, Barcelona, Spain

Luis L. Bonilla
Universidad Carlos III de Madrid, Escuela Politécnica Superior, 28913 Leganés, Madrid, Spain

Michael J. Bergmann and Stephen W. Teitsworth
Department of Physics, Box 90305, Duke University, Durham, North Carolina 27708-0305
(Received 16 July 1993)

Numerical-simulation results are presented for a simple drift-diffusion model which describes time-dependent and nonlinear electrical transport properties of extrinsic semiconductors under time-independent (dc) voltage bias. Simulations for finite-length samples with Ohmic boundary conditions yield dynamically stable solitary space-charge waves that travel periodically across the sample. Numerical estimates of wave speed, the wave size, and onset phenomena are in excellent agreement with recent experiments in p-type germanium.

Spatiotemporal instabilities have recently been reported in voltage-biased samples of liquid-helium-cooled crystals of ultrapure p-type Ge.[1-5] For applied dc voltages in excess of the impurity breakdown value, high-field domains are observed to nucleate and cross the sample, giving rise to periodic current oscillations. Such solitary-wave phenomena have been employed as the basis for studies of temporal and spatiotemporal chaos in experiments which are subjected to an additional ac voltage bias.[3] However, a theoretical understanding of the physical origin of these solitary waves has been lacking. In addition to p-type Ge,[1-6] spontaneous current instabilities due to trapping effects have also been observed in other semiconductors at low temperature including GaAs, InSb, and Si.[7-9] In this paper we present numerical and analytical evidence which strongly supports use of a simple "reduced equation" model that successfully explains *in detail* many observed features of the domain dynamics in Ge under dc voltage bias, with the expectation that an exhaustive explanation of related phenomena—including spatiotemporal chaotic behavior—might be built upon it.

Our work is based on a drift-diffusion model with ionizable impurities and mobile carriers.[10,11] The model features a negative differential impact ionization coefficient that gives rise to an effective negative differential resistance which causes the instability. For Ge, the dielectric relaxation time (~ 1 ns) is much shorter than the characteristic time for impact ionization or recombination on the shallow impurities ($\sim$several μs) which, in turn, is much shorter than the diffusion time for the carriers ($\sim$several ms).[12] This separation of time scales allows us to simplify the drift-diffusion model to the following dimensionless reduced equation for the electric field $E(x,\tau)$ and the current $J(\tau)$:[12,13]

$$\frac{\partial^2 E}{\partial x\,\partial \tau}+c_1(E,J)\frac{\partial E}{\partial \tau}+c_2(E,J)\frac{\partial E}{\partial x}+c_3(E,J)=V(E)^{-1}\frac{dJ}{d\tau} \tag{1a}$$

and

$$\int_0^L E(x,\tau)dx=\phi\ , \tag{1b}$$

where

$$c_1(E,J)=JV'(E)/V(E)^2\ , \tag{1c}$$

$$c_2(E,J)=J[K(E)+R(E)]/V(E)\ , \tag{1d}$$

and

$$c_3(E,J)=\left[\left\{\frac{\alpha K(E)}{K(E)+R(E)}-1\right\}V(E)-J\right]\frac{c_2(E,J)}{V(E)}\ . \tag{1e}$$

Equation (1a) applies for electric fields above the threshold for impurity breakdown, where photogeneration terms can be ignored.[13] The coefficients $V(E)$, $K(E)$, and $R(E)$ are the field-dependent carrier velocity, impact ionization, and recombination coefficients, respectively; their physical basis has been discussed extensively,[14,15] and numerical forms used in this paper are plotted in Fig. 1. In Fig. 1(c) we also plot the steady-state solution J vs E of Eqs. (1a)–(1d) defined by $c_3(E,J)=0$. The parame-

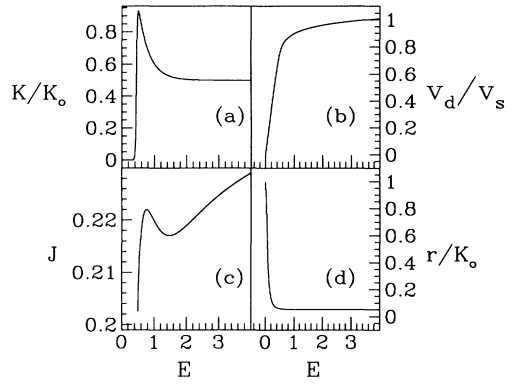

FIG. 1. Nondimensional transport quantities: (a) drift velocity V vs electric field E; (b) impact ionization coefficient K vs E; (c) the J-E curve; and (d) capture coefficient R vs E.

ter α (≥ 1) is the impurity compensation ratio (i.e., the residual shallow acceptor concentration divided by the residual donor concentration; it is close to 1 in the experiments of Refs. 3–5) and ϕ is the nondimensional dc voltage bias. Expressions for the nondimensional quantities used here in terms of dimensional ones have been given in detail elsewhere;[12] the unit of length corresponds to ~ 0.013 mm, time $\sim 3\times 10^{-6}$ s, electric field ~ 10 V/cm, and current density ~ 60 mA/cm^2.

Equations (1a) and (1b) are to be solved with appropriate initial conditions and the following Ohmic boundary condition at the injecting contact:

$$E(x=0,\tau)=\rho_0 J(\tau)\ . \tag{2}$$

We have assumed that the contact has a dimensionless resistivity $\rho_0>0$. This boundary condition is a simple phenomenological current-field characteristic curve used in previous studies,[13–16] and the results obtained with it can easily be extended to nonlinear metal-semiconductor characteristic curves.[17–19] The reduced model Eqs. (1) and (2) is expected to be a good approximation of the full drift diffusion model except in a very narrow boundary layer near the receiving contact at $x=L$, where the electric field changes abruptly to satisfy an Ohmic boundary condition of the same form as Eq. (2). The dimensionless semiconductor length L corresponding to experimental p-Ge samples is very large (estimated to be 1150 for Ref. 4).

We have performed a series of numerical simulations of Eqs. (1) and (2) with numerical values of the parameters corresponding to p-Ge experiments ($\alpha=1.35$, $L=1150$, and $\rho_0=4.0$). Simulations were performed on a Sun SPARC workstation (model ELC) and incorporated a Newton's-method routine which adjusts the current $J(\tau)$ to maintain the global constraint Eq. (1b). Results are shown in Figs. 2 and 3. Figure 2 corresponds to an average field $\phi/L=0.7599$ (just above the field $\phi_\alpha/L=0.7480$, for which the steady state becomes unstable); notice that the current oscillation in Fig. 2(b) is due to the nucleation and propagation of small waves whose amplitudes decay as they move into the sample, so that they disappear before reaching the receiving contact. Such behavior is also observed in the experiments of

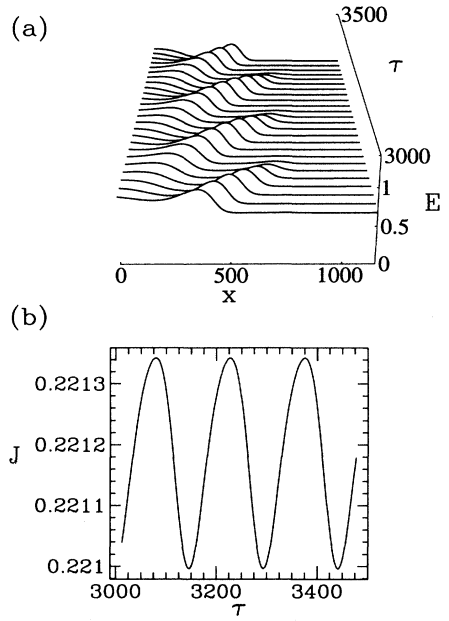

FIG. 2. (a) Spatial form of electric field vs position and time for $\phi/L=0.7599$; (b) corresponding current $J(\tau)$.

Kahn, Mar, and Westervelt.[5] Figure 3 corresponds to a slightly larger voltage $\phi/L=0.7605$ where the current oscillations are due to solitary-wave dynamics. Thus far from the contacts a solitary wave moves with constant speed and the current has a flat interval. When the wave arrives at $x=L$, it starts disappearing and $J(\tau)$ increases until it surpasses a critical value J_c defined by $c_3(\rho_0 J_c, J_c)=0$ [i.e., the straight line $J=E/\rho_0$ cuts the steady-state curve $J=J(E)$ at $E=E_c$ where E_c is in the negative differential part of the $J(E)$ curve]. At the same

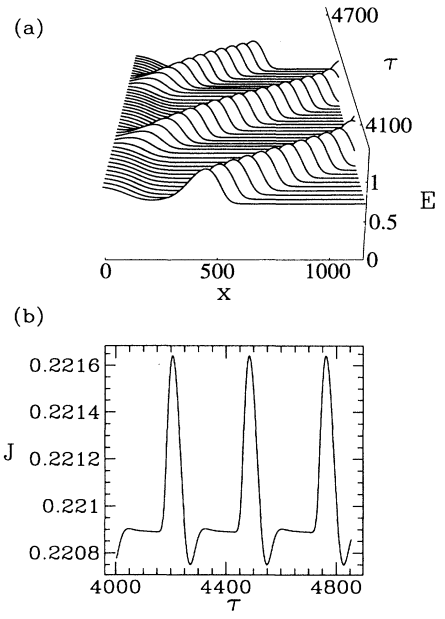

FIG. 3. (a) Spatial form of electric field vs position and time for $\phi/L=0.7605$; (b) corresponding current $J(\tau)$.

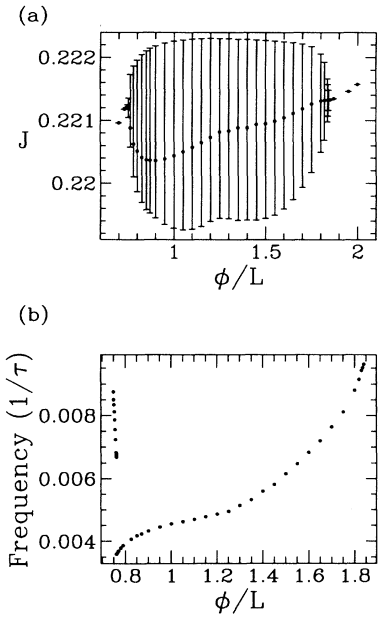

FIG. 4. (a) Bifurcation diagram showing time-averaged J vs ϕ/L. (b) Fundamental oscillation frequency for $J(\tau)$ vs ϕ/L.

time a small solitary wave is created at the injecting contact and begins to move toward $x=L$, gaining all the area lost by the dying wave, while the current diminishes. When the wave at $x=L$ has disappeared completely, the other solitary wave has reached maturity and the process repeats itself. For voltages just below $\phi_\omega/L=1.84$ (the voltage above which the steady state is again stable), the solitary-wave dynamics are very similar, although the waves are almost as wide as the entire sample.

Our numerical results can be interpreted theoretically with the help of the global bifurcation diagram (current averaged over one period versus dc voltage) shown in Fig. 4(a). Figure 4(b) shows the fundamental frequency of the current vs dc voltage and clearly indicates an abrupt jump at $\phi_\beta/L=0.7601>\phi_\alpha/L$ which corresponds to the transition from the decaying periodic waves of Fig. 2 to the fully developed solitary waves of Fig. 3. This transition is slightly hysteretic (not visible on the scale of Fig. 4) and—when coupled with low level noise typically found in experiments—it might be expected to produce intermittent transitions between the damped and traveling waves as observed in experiments near the onset regime.[4] Outside this narrow hysteretic region, Eqs. (1) and (2) have unique periodic solutions for given values of dc voltage. For voltages outside the interval $(\phi_\alpha,\phi_\omega)$ the time-independent steady state is always stable. Inside $(\phi_\alpha,\phi_\omega)$ the electric current $J(\tau)$ is periodic, but its frequency and shape and also the spatial profile of the electric field change according to the voltage (Figs. 2–4). For long semiconductors ($L\gg1$) we have[13]

$$\phi_\alpha=E_1L+(E_2-E_1)[V(E_2)/\sigma(E_2)]\ln(L)\ ,$$
$$\sigma(E)\equiv|dj/dE|\ . \tag{3}$$

Here $E_1(J)\le E_2(J)\le E_3(J)$ are the three solutions of $c_3(E,J)=0$, calculated at $J=J_c$. The simulations of Eqs. (1) and (2) give a value of onset of $\phi_\alpha=860$, and this agrees quite closely with the value obtained by direct evaluation of Eq. (3). For L, $\ln(L)\gg1$, and voltages between $E_1(J_c)L$ and $E_2(J_c)L$ the profile of the stationary (but position-dependent) field can be approximated by a step function $E(x)=E_2(J_c)$ for $0<x<\Delta x$, and $E(x)=E_1(J_c)$ for $\Delta x<x<L$, where

$$\Delta x=[\phi-E_1(J_c)L]/[E_2(J_c)-E_1(J_c)]\ . \tag{4}$$

We can linearize Eqs. (1) and (2) about this approximate stationary field and take $J=J_c$. We then solve the resulting equations with a separation of variables ansatz[13]

$$E(x,\tau)=E(x)+e^{\lambda\tau}\hat{e}(x)\ . \tag{5}$$

The resulting expressions can be simplified in the limit $L\to+\infty$. We find that

$$\lambda=i(2n+1)\frac{\pi\sigma_2J_c(K_2+R_2)}{(V_2\sigma_2+J_cV_2')\ln(L)}\ ,$$
$$\{n=0,\pm1,\ldots,O[\ln(L)]\}\ , \tag{6a}$$

with

$$\Delta x=\frac{V_2}{\sigma_2}\ln\left\{\frac{\sigma_2^2L}{(1+\rho_0)(V_1\sigma_2+V_2\sigma_1)}\right\}\ . \tag{6b}$$

In Eqs. (6a) and (6b) the subscripts 1 and 2 mean that the corresponding functions are to be evaluated at $E_1(J_c)$ and $E_2(J_c)$, respectively. Equation (6a) shows that there are many modes that become unstable for voltages larger than ϕ_α in the limit $L\to\infty$. The main conclusion of this analysis is that for voltages just above ϕ_α, and for $\ln(L)\to\infty$, the electric field has a profile similar to that of the steady state but with traveling waves of period $2\Delta x$ (and amplitude exponentially growing with x) which move with $O(1)$ velocity on the high-field portion of $E(x)$. For $\Delta x<x<L$, the field difference with the steady state decreases exponentially with $(x-\Delta x)$. Due to Eq. (2), the current is a periodic function of time centered about J_c. Since the period of the oscillation is $2\Delta x$, there is typically one "solitary wave" moving from $x=0$ and another one being created behind it. The wave reaches its maximum size at $x\approx\Delta x$ and is then attenuated as it proceeds further. This situation is similar to that shown by the numerical simulations for voltages near ϕ_α (Fig. 2). As the voltage grows, so does the amplitude of the current oscillation and of the waves which penetrate more deeply into the attenuation region $\Delta x<x<L$ (while still reaching their maximum size at $x\approx\Delta x$), as one may expect from the linear stability analysis of the steady state.[13,20]

The previous pattern of the oscillations continues until the abrupt drop of the average current at the transition voltage ϕ_β. For voltages between ϕ_α and ϕ_β, we say that the oscillation of the current is typical of the "onset region" of the instability, because its character can be extrapolated from an analysis of the bifurcation at $\phi=\phi_\alpha$. The frequency dependence of such a region is apparently also experimentally observed in long p-Ge samples.[4,5] For larger voltages, the oscillations of the current are

produced by the dynamics of the traveling solitary waves. We call the region $(\phi_\beta, \phi_\omega)$ the "solitary-wave region" for this reason. We conjecture that ϕ_β is of the order of magnitude of the minimum voltage for which a solitary wave detached from the contacts can be stable. In the onset region the solitary waves are too small to be stable and thus decay as they move through the attenuation region of the semiconductor.

A strikingly similar bifurcation scenario near the onset has recently been reported for a standard drift-diffusion model of the Gunn effect in GaAs.[19–21] This similarity is surprising because the dynamical equations for the Gunn effect and Eq. (1)—as well as the microscopic mechanism underlying the respective instabilities—are of fundamentally different character. Thus the Gunn effect is described by a partial differential equation of parabolic type,[19] and results from negative differential carrier mobility associated with very rapid intervalley transfer, whereas Eq. (1) for p-Ge is hyperbolic and the instability mechanism in p-Ge is due to negative differential trapping on impurities (via relatively slow hole capture or impact ionization processes). In both cases a crucial role appears to be played by the constant voltage constraint Eq. (1b) and the Ohmic boundary condition Eq. (2).

The region near $\phi=\phi_\omega$ can be analyzed in the same way as the onset region and will be discussed in a future paper. We emphasize that our simulations considered a $J(E)$ [Fig. 1(c)] curve that has two positive extrema and an injecting contact with a relatively high resistivity. Thus different phenomena should be expected for other contact resistivities. For instance, we have numerically observed current oscillations caused by traveling electric *monopole* dynamics for low-resistivity contacts, i.e., $0<\rho_0<\rho_{0M}$.[22]

Comparison to available experimental data shows excellent agreement with most of the dynamical properties of the solitary waves. Nonetheless, several interesting questions remain. For example, does the hysteretic transition at ϕ_β quantitatively explain experimentally observed intermittency phenomena[4,5] when a reasonable experimental noise term is added? Another open question is whether or not temporal and even spatiotemporal chaotic behavior observed for ac+dc bias experiments will be captured by the "reduced" model Eqs. (1) and (2); work in this direction is currently in progress.

We acknowledge helpful discussions with A. M. Kahn, D. J. Mar, and R. M. Westervelt about the experimental data, and with Francisco Higuera and José Vega on numerical and analytical techniques. We also wish to acknowledge the support of the National Science Foundation through Grant No. DMR-9157539, the DGICYT under Grant No. PB89-0629, and the NATO Travel grant program.

[1]S. W. Teitsworth, R. M. Westervelt, and E. E. Haller, Phys. Rev. Lett. **51**, 825 (1983).
[2]E. G. Gwinn and R. M. Westervelt, Phys. Rev. Lett. **57**, 1060 (1986); **59**, 247(E) (1987).
[3]A. M. Kahn, D. J. Mar, and R. M. Westervelt, Phys. Rev. Lett. **68**, 369 (1992).
[4]A. M. Kahn, D. J. Mar, and R. M. Westervelt, Phys. Rev. B **43**, 9740 (1991).
[5]A. M. Kahn, D. J. Mar, and R. M. Westervelt, Phys. Rev. B **45**, 8342 (1992).
[6]J. Peinke, A. Mühlbach, R. P. Huebener, and J. Parisi, Phys. Lett. A **108**, 407 (1985).
[7]K. Aoki and K. Yamamoto, Phys. Lett. A **98**, 72 (1983).
[8]D. G. Seiler, C. L. Littler, R. J. Justice, and P. W. Milonni, Phys. Lett. A **108**, 462 (1985).
[9]K. Yamada, N. Takara, H. Imada, N. Miura, and C. Hamaguchi, Solid State Electron. **31**, 809 (1988).
[10]S. W. Teitsworth and R. M. Westervelt, Phys. Rev. Lett. **53**, 2587 (1984).
[11]S. W. Teitsworth, Appl. Phys. A **48**, 127 (1989).
[12]L. L. Bonilla and S. W. Teitsworth, Physica D **50**, 545 (1991).
[13]L. L. Bonilla, Phys. Rev. B **45**, 11 642 (1992).
[14]R. M. Westervelt and S. W. Teitsworth, J. Appl. Phys. **57**, 5457 (1985).
[15]L. Regianni and V. Mitin, Nuovo Cimento **12**, 1 (1989).
[16]L. L. Bonilla, Physica D **55**, 182 (1992).
[17]H. Kroemer, IEEE Trans. Electron Devices **ED-15**, 819 (1968).
[18]H. L. Grubin, IEEE Trans. Electron Devices **ED-23**, 1012 (1976).
[19]F. J. Higuera and L. L. Bonilla, Physica D **57**, 161 (1992).
[20]L. L. Bonilla and F. J. Higuera (unpublished).
[21]H. L. Grubin, M. P. Shaw, and P. R. Solomon, IEEE Trans. Electron Devices **ED-20**, 63 (1973).
[22]M. J. Bergmann and S. W. Teitsworth (unpublished).